ACS APPLIED ENERGY MATERIALS
Cite This: ACS Appl. Energy Mater. 2019, 2, 3017−3020
Letter
www.acsaem.org

# Lead Oxide Microparticles Coated by Ethylenediamine-Cross-Linked Graphene Oxide for Lithium Ion Battery Anodes

Alan Guo,[†] Eric Chen,[‡] Bryan R. Wygant,[†] Adam Heller,[‡] and C. Buddie Mullins*[,†,‡,§,∥]

[†]Department of Chemistry, [‡]McKetta Department of Chemical Engineering, [§]Texas Materials Institute, and [∥]Center for Electrochemistry, University of Texas at Austin, Austin, Texas 78712-1589, United States

Supporting Information

**ABSTRACT:** Lead-based anodes in Li-ion batteries have potential in stationary storage applications, due to their high theoretical volumetric energy density. In this study, the cycle performance of PbO was improved by coating it with a network of graphene oxide sheets, cross-linked by ethylenediamine. The carbon coating reduced electrode capacity degradation from 0.42% to 0.22% per cycle over 200 cycles, increased Coulombic efficiency from 96% to 99%, and increased the accessible capacity of the electrodes through improved electrical connectivity. This low-temperature carbon coating technique is potentially advantageous to other metastable and low-melting electroactive materials.

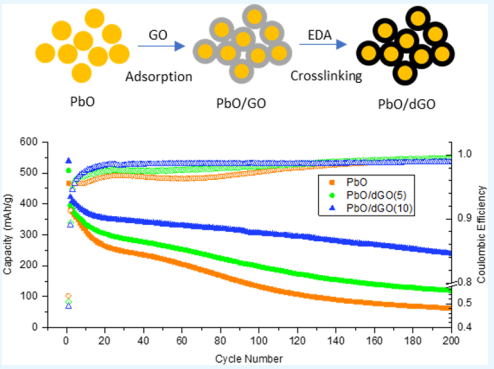


**KEYWORDS:** *lithium-ion batteries, lead oxide, microparticles, graphene oxide, carbon coating*



Anode materials with high volumetric energy densities are highly advantageous in stationary applications, such as grid storage. The theoretical volumetric energy densities of alloying Group IV elements far surpass that of graphite, as they can to store up to 4.4 Li atoms per M (M = Si, Ge, Sn, Pb), compared to only 0.17 Li atoms per graphite carbon atom.[1] Because of its high gravimetric energy density (3579 mAh/g), silicon has been extensively investigated as the successor to graphite. While the theoretical gravimetric energy density of lead (453 mAh/g) is much lower, its theoretical volumetric specific capacity of 1937 Ah/L rivals that of silicon, 2194 Ah/L, and is much higher than that of graphite, 719 Ah/L.[1,2] In a typical 52 Ah graphite/NCM pouch cell, the anode occupies approximately 31% of the volume.[3] In turn, a lead-based anode can potentially reduce the volume of the cell by as much as 20%. Furthermore, lead electrodes offer a fully developed recycling infrastructure with >99% recovery and reuse of Pb in North America, primarily applied in the recycling of lead acid batteries in automobiles.[4]

The challenge of Group IV Li-battery anodes, including lead anodes, is their 300% volume expansion upon lithiation.[1] It leads to particle pulverization, loss of electrical contact with the current collector, and continuous parasitic side reactions of newly exposed active material surfaces with the electrolyte, all contributing to the observed rapid capacity loss.[1,5] A common way to mitigate these issues is carbon coating, which buffers volume expansion and passivates the particle surfaces to prevent additional parasitic side reactions.[6−8] However, conformal carbon coating typically involves pyrolysis above 800 °C, much higher than the melting point of lead, 327 °C. Although carbon composites have been created from precursors of tin[9,10] and lead,[11,12] the carbon was not conformal to the active material, thereby negating some of the important benefits of carbon coating. In this study, a conformal coating was applied to PbO particles at mild temperature, where the product $Li_2O$ upon initial lithiation has been shown to stabilize the cycling of Group IV anodes.[12,13]

Reduced graphene oxide (rGO) has been previously demonstrated as a conformal carbon coating on sulfur cathode particles, in order to reduce sulfur shuttling.[14,15] Furthermore, chemical cross-linking and reduction of graphene oxide (GO) to rGO using ethylenediamine (EDA) has been previously claimed.[16,17] In this study, PbO particles were coated using GO sheets, which were subsequently functionalized and cross-linked with EDA, in order to form a cross-linked GO-derived coating, abbreviated dGO (Figure 1). To do so, aqueous solutions of PbO and GO were prepared separately. Upon mixing, a stable PbO/GO colloid formed, which is supported

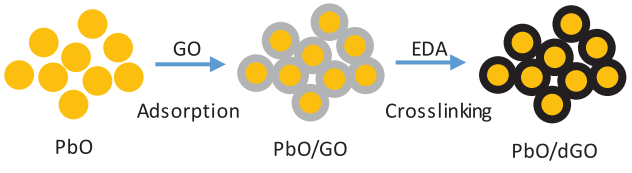


**Figure 1.** Schematic of the synthesis of PbO/dGO by adsorbing GO onto PbO, followed by treatment with EDA.

**Received:** February 26, 2019
**Accepted:** April 11, 2019
**Published:** April 11, 2019




DOI: 10.1021/acsaem.9b00401
ACS Appl. Energy Mater. 2019, 2, 3017−3020

by strong adsorption between PbO and GO.[18,19] EDA was subsequently added in excess, at a 2:1 EDA:GO molar ratio, and left to stir for 24 h at 80 °C, in order to form a cross-linked dGO network. Details of the material synthesis can be found in the Supporting Information.

The XRD scan shown in Figure 2a confirms PbO as the active material, accompanied by weak signals of plumbonacrite

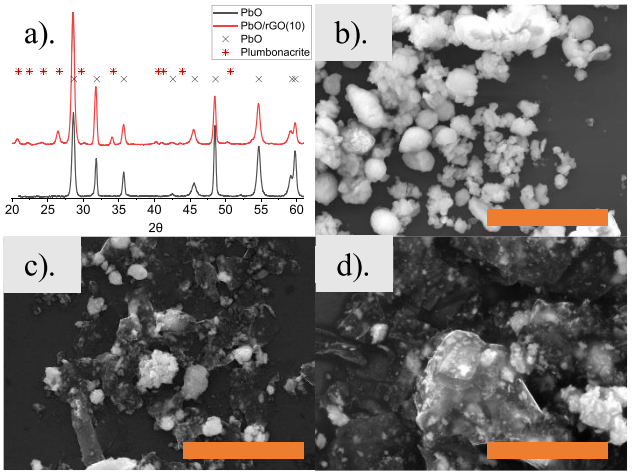


**Figure 2.** (a) XRD scans of PbO and PbO coated by 10 wt % dGO, and SEM images of the (b) PbO microparticles, (c) PbO with 5 wt % dGO coating, and (d) PbO with 10 wt % dGO coating. Scale bars for all images represent 10 $\mu$m.

or lead oxide carbonate hydroxide ($Pb_{10}(CO_3)_6(OH)_{10}O$), after coating with dGO.[20,21] Panels b–d of Figure 2 show the PbO particles, as well as PbO particles that have been coated by 5 and 10 wt % dGO. EDS scans shown in Figure S-1 confirm the presence of PbO (Pb and O), dGO (C), and a faint signal of EDA reaction products with GO (N).

The FTIR spectrum of GO without PbO (Figure 3a) shows prominent carbonyl (C═O), aromatic (C═C), carboxy (C–

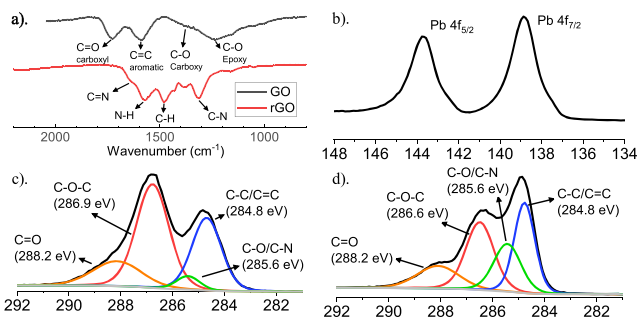


**Figure 3.** (a) FTIR spectrum of GO and dGO (without PbO); XPS analysis of Pb 4f (b) and C 1s of GO (c) and dGO (d).

O), and epoxy (C–O) groups, at wave numbers 1727, 1588, 1342, and 1234 $cm^{-1}$, respectively. By contrast, FTIR of the dGO (also without PbO) shows reduced carboxyl and epoxy signals, in favor of imine (C═N), amine (N–H), carbon–hydrogen (C–H), and carbon–nitrogen (C–N) signals at wavenumbers 1640, 1569, 1480, and 1311 $cm^{-1}$, respectively.[22,23] XPS survey scans indicate that the C:O ratio of the GO increased from 2.3:1 to 3.2:1 after reaction with EDA. XPS scans of Pb 4f (Figure 3b) confirm the Pb(II) oxidation state.[24] Scans of the C 1s regions for GO and dGO (Figure 3c,d) show C–C/C═C, C–O/C–N, C–O–C, and C═O peaks at 284.8, 285.6, 286.9, and 288.2 eV.[23,25] The substitution of epoxy C–O–C bonds by C–O/C–N bonds is consistent with reaction of EDA amines and epoxy functions on the GO, forming C–OH and C–N–R bonds.[16] Cross-linking occurs when epoxy functions on proximal GO sheets are bound by EDA. Additionally, heat-assisted reaction between EDA and carboxyl groups forms amides (O═C–N) on the edge of the GO sheets, also leading to potential GO cross-linking. The loss of oxygen in GO by EDA, indicated by the increase in C/O ratio, has been attributed to EDA-assisted dehydration, after it has reacted with epoxy groups on the GO sheets.[17] The substitution of oxygen by nitrogen in carbonyl and carboxyl groups can also lead to an increased C/O ratio and, consequently, improvement in electrical conductivity.

During electrode fabrication, active material (AM) to conductive additive (CA) to binder weight ratios were kept constant at 80:12:8 for uncoated PbO, 84:8:8 for PbO coated by 5 wt % dGO, and 88:4:8 for PbO coated by 10 wt % dGO, abbreviated as PbO, PbO/dGO(5), and PbO/dGO(10), respectively. This maintains the same active material loading for all electrodes. PbO mass loadings for these electrodes were kept between 1.2 and 1.3 $mg/cm^2$. Electrode thicknesses averaged 9.3 $\mu$m prior to lithiation and 15.3 $\mu$m after lithiation. Further details of these procedures can be found in the Supporting Information.

Cyclic voltammograms of PbO and PbO/dGO(10) electrodes cycled between 0.01 and 2.0 V vs $Li/Li^+$ at 0.1 mV/s scan rate (Figure 4a,b) show irreversible lithium reduction of PbO to Pb and $Li_2O$ between 1.0 and 2.0 V. This initial reduction was accompanied by an intermediate transition of $Pb^{2+}$ to $Pb^+$ (~1.5 V vs $Li/Li^+$), followed by the transition of $Pb^+$ to Pb (~1.3 V vs $Li/Li^+$).[12] Reversible Pb lithiation peaks were observed between 0.01 and 1.0 V vs $Li/Li^+$, with a larger

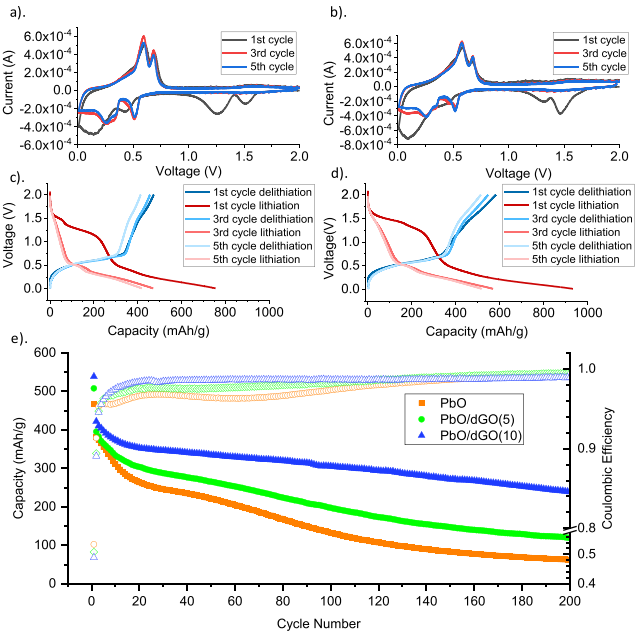


**Figure 4.** Cyclic voltammetry at 0.1 mV/s between 0.01 and 2 V of (a) PbO electrode and (b) PbO/dGO(10) electrode. Charge/discharge profiles of the first five cycles of (c) PbO and (d) PbO/dGO(10). (e) Long-term cycling of PbO, PbO/dGO(5) and PbO/dGO(10), with a C/20 formation cycle, followed by C/2 cycling



DOI: 10.1021/acsaem.9b00401
ACS Appl. Energy Mater. 2019, 2, 3017–3020

background current during the first cycle, implying parasitic reactions associated with the formation of the solid electrolyte interface (SEI). This irreversible reaction is also observed in the charge/discharge voltage profiles of PbO and PbO/dGO(10) half-cells during the first five cycles (Figure 4c,d).

Half-cells containing PbO, PbO/dGO(5), and PbO/dGO(10) were cycled at *C*/2 for 200 cycles (Figure 4e). The calculated *C*-rates were based on the 420 mAh/g capacity of lead oxide lithiated to $Li_{3.5}Pb$.[26] During their initial *C*/20 formation cycles, PbO, PbO/dGO(5), and PbO/dGO(10) had average capacities of 468, 508, and 539 mAh/g, respectively. In the *C*/2 cycles, the initial capacities were respectively 383, 395, and 422 mAh/g for PbO, PbO/dGO(5), and PbO/dGO(10), with capacity fade averaging 0.42%, 0.35%, and 0.22% per cycle over 200 cycles. The respective Coulombic efficiencies (CE) improved with increasing dGO content, plateauing near 96%, 97.6%, and 99% after ∼80 cycles. The overall increase in CE after 80 cycles is attributed to the higher effective *C*-rates, due to the decrease in the electrode capacities. The improvements in capacity retention and CE with increased dGO content are attributed to improved buffering capacity of the carbon coating. Further optimization of the carbon coating can be made by varying characteristics of the GO precursor, such as size and degree of oxidation—also functionality. Amine-functionalized polymers of different sizes and viscoelasticities can be tested to fine-tune the elasticity of the carbon coating, improving its ability to accommodate repeated volume expansions. Additionally more powerful chemical reducing agents can be used to increase the C/O ratio of the carbon coating and improve its electrical conductivity.

As seen in Figure 2, the conformal dGO fully encapsulates the electroactive particles and also bridges multiple particles. This encapsulation provides electrical continuity, which would in turn be superior to using conductive carbon additives such as Super P, which contacts only portions of the active material surfaces and is more prone to breaks in electrical contact under the stresses of expansion/contraction of repeated lithiation cycles. Scanning electron microscopy (SEM) images of the morphologies of the electrodes before and after cycling for PbO and PbO/dGO(10) can be found in Figures S-4 and S-5, respectively. Figure S-4b shows that not all the particles were enveloped by the Super P carbon additives, in contrast to Figure S-5b, where all of the particles were enveloped by dGO. The exposed particle surfaces led to excess SEI formation in the PbO electrode after 200 cycles (Figure S-4c,d), leading to larger aggregates of particles surrounded by SEI. By contrast, the PbO/dGO(10) electrode after 200 cycles (Figure S-5c,d) shows improvement in retaining morphologies of individual PbO particles, indicating reduced SEI formation, as a result of full particle encapsulation by dGO. The conformal carbon coating also buffers the particle's volume change during cycling and helps maintain the mechanical structure of the electrode.[1] Furthermore, the encapsulating carbon coating effectively insulates the active material from further reactions with the electrolyte, limiting SEI growth and improving the CE.

Super P (SP) has been shown to provide up to 150 mAh/g in excess capacity.[27] In turn, the excess capacity of the dGO was also determined and compared to that of SP, by cycling electrodes containing dGO (or SP), with equal amounts of carboxymethylcellulose (CMC) binder (details can be found in the Supporting Information). Figure S-2 shows reversible capacities of the SP and dGO electrodes at current densities of 20, 50, 100, 200, 500, 1000, and 50 mA/g. The average respective capacities were 195, 148, 110, 78, 47, 31, and 141 mAh/g for SP and only 4.7, 3.4, 2.5, 1.9, 1.3, 0.9, and 2.9 mAh/g for dGO. Since the *d*-spacing between restacked dGO sheets separated by EDA molecules is 0.90 nm,[16] compared to 0.14 nm for graphite, dGO serves as a poor host structure for $Li^+$ intercalation. Consequently, the specific capacities of SP in the PbO, PbO/dGO(5), and PbO/dGO(10) electrodes at *C*/2 (Figure 4e) are estimated to be 11.5, 7.7, and 3.9 mAh/g, respectively. The contribution of dGO is estimated to be only <0.2 mAh/g for PbO/dGO(10) and <0.1 mAh/g for PbO/dGO(5).

In conclusion, at low temperature, an aqueous carbon coating technique was developed by adsorbing GO onto PbO microparticles and cross-linking the GO to form a dGO coating. The coating increased the capacity of the electrodes, by providing better electrical connectivity than traditional conductive particle additives, reduced the capacity fade from 0.42% to 0.22% per cycle, and raised Coulombic efficiency from 96% to 99%. This novel coating technique in principle can also be applied to other GO adsorbing materials for Li and Na batteries.

## ■ ASSOCIATED CONTENT

### Supporting Information

The Supporting Information is available free of charge on the ACS Publications website at DOI: 10.1021/acsaem.9b00401.

Detailed procedure of material synthesis, electrode fabrication and electrode characteristics, EDS analysis of PbO/dGO, lithiation capacities of Super P and dGO, complete coin cell cycling data of PbO, PbO/dGO(5), and PbO/dGO(10), and electrode morphology analysis before and after cycling of PbO and PbO/dGO(10) (PDF)

## ■ AUTHOR INFORMATION


### Corresponding Author

*E-mail: mullins@che.utexas.edu.

### ORCID

Adam Heller: 0000-0003-0181-1246

C. Buddie Mullins: 0000-0003-1030-4801


### Notes

The authors declare no competing financial interest.

## ■ ACKNOWLEDGMENTS

We acknowledge the generous support provided by the Welch Foundation (via Grants F-1131 (A.H.) and F-1436 (C.B.M.)) as well as the National Science Foundation via Grant CBET-1603491. We also thank Celgard Corp. for their provision of separators, and Solvay Fluor for their donation of fluoroethylene carbonate.

## ■ REFERENCES

(1) Obrovac, M. N.; Chevrier, V. L. Alloy negative electrodes for Li-ion batteries. *Chem. Rev.* **2014**, *114*, 11444−11502.

(2) Louli, A. J.; Li, J.; Trussler, S.; Fell, C. R.; Dahn, J. R. Volume, Pressure and Thickness Evolution of Li-Ion Pouch Cells with Silicon-Composite Negative Electrodes. *J. Electrochem. Soc.* **2017**, *164*, A2689−A2696.

(3) Nykvist, B.; Nilsson, M. Rapidly falling costs of battery packs for electric vehicles. *Nat. Clim. Change* **2015**, *5*, 329−332.



DOI: 10.1021/acsaem.9b00401
*ACS Appl. Energy Mater.* 2019, 2, 3017−3020

(4) Jolly, R.; Rhin, C. The recycling of lead-acid batteries: production of lead and polypropylene. *Resour. Conserv. Recycl.* **1994**, *10*, 137−143.
(5) Tian, H.; Xin, F.; Wang, X.; He, W.; Han, W. High capacity group-IV elements (Si, Ge, Sn) based anodes for lithium-ion batteries. *J. Mater.* **2015**, *1*, 153−169.
(6) Zhou, X. Y.; Tang, J. J.; Yang, J.; Xie, J.; Ma, L. L. Silicon@ carbon hollow core-shell heterostructures novel anode materials for lithium ion batteries. *Electrochim. Acta* **2013**, *87*, 663−668.
(7) Tokur, M.; et al. Closing to Scaling-Up High Reversible Si/rGO Nanocomposite Anodes for Lithium Ion Batteries. *Electrochim. Acta* **2016**, *216*, 312−319.
(8) Xue, L.; et al. Carbon-Coated Si Nanoparticles Dispersed in Carbon Nanotube Networks As Anode Material for Lithium-Ion Batteries. *ACS Appl. Mater. Interfaces* **2013**, *5*, 21−25.
(9) Li, S.; et al. Comparison of Si/C, Ge/C and Sn/C composite nanofiber anodes used in advanced lithium-ion batteries. *Solid State Ionics* **2014**, *254*, 17−26.
(10) Ai, W.; et al. Surfactant-assisted encapsulation of uniform SnO2 nanoparticles in graphene layers for high-performance Li-storage. *2D Mater.* **2015**, *2*, 014005.
(11) Pan, Q.; Wang, Z.; Liu, J.; Yin, G.; Gu, M. PbO@C core-shell nanocomposites as an anode material of lithium-ion batteries. *Electrochem. Commun.* **2009**, *11*, 917−920.
(12) Li, C.-H.; Sengodu, P.; Wang, D.-Y.; Kuo, T.-R.; Chen, C.-C. Highly stable cycling of a lead oxide/copper nanocomposite as an anode material in lithium ion batteries. *RSC Adv.* **2015**, *5*, 50245−50252.
(13) Abel, P. R.; Lin, Y. M.; Celio, H.; Heller, A.; Mullins, C. B. Improving the stability of nanostructured silicon thin film lithium-ion battery anodes through their controlled oxidation. *ACS Nano* **2012**, *6*, 2506−2516.
(14) Wang, Z.; Dong, Y.; Li, H.; Zhao, Z.; Bin Wu, H.; Hao, C.; Liu, S.; Qiu, J.; Lou, X. W. D.; et al. Enhancing lithium-sulphur battery performance by strongly binding the discharge products on amino-functionalized reduced graphene oxide. *Nat. Commun.* **2014**, *5*, 5002.
(15) Wang, H.; et al. Graphene-wrapped sulfur particles as a rechargeable lithium-sulfur battery cathode material with high capacity and cycling stability. *Nano Lett.* **2011**, *11*, 2644−2647.
(16) Hung, W. S.; et al. Cross-linking with diamine monomers to prepare composite graphene oxide-framework membranes with varying d-spacing. *Chem. Mater.* **2014**, *26*, 2983−2990.
(17) Che, J.; Shen, L.; Xiao, Y. A new approach to fabricate graphene nanosheets in organic medium: Combination of reduction and dispersion. *J. Mater. Chem.* **2010**, *20*, 1722−1727.
(18) Madadrang, C. J.; et al. Adsorption behavior of EDTA-graphene oxide for Pb (II) removal. *ACS Appl. Mater. Interfaces* **2012**, *4*, 1186−1193.
(19) Olanipekun, O.; Oyefusi, A.; Neelgund, G. M.; Oki, A. Adsorption of lead over graphite oxide. *Spectrochim. Acta, Part A* **2014**, *118*, 857−860.
(20) Perry, D. L.; Wilkinson, T. J. Synthesis of high-purity $\alpha$- And $\beta$-PbO and possible applications to synthesis and processing of other lead oxide materials. *Appl. Phys. A: Mater. Sci. Process.* **2007**, *89*, 77−80.
(21) Urbiola, I. R. C.; et al. Combined CBD-CVD technique for preparation of II-VI semiconductor films for solar cells. *Energy Procedia* **2014**, *57*, 24−31.
(22) Zhang, J.; Xu, Y.; Liu, Z.; Yang, W.; Liu, J. A highly conductive porous graphene electrode prepared via in situ reduction of graphene oxide using Cu nanoparticles for the fabrication of high performance supercapacitors. *RSC Adv.* **2015**, *5*, 54275−54282.
(23) Jia, Z.; Wang, Y. Covalently crosslinked graphene oxide membranes by esterification reactions for ions separation. *J. Mater. Chem. A* **2015**, *3*, 4405−4412.
(24) Leelavathi, A.; Mukherjee, B.; Nethravathi, C.; Kundu, S.; Dhivya, M.; Ravishankar, N.; Madras, G. Highly photoactive heterostructures of PbO quantum dots on $TiO_2$. *RSC Adv.* **2013**, *3*, 20970−20977.
(25) Yang, D.; et al. Chemical analysis of graphene oxide films after heat and chemical treatments by X-ray photoelectron and Micro-Raman spectroscopy. *Carbon* **2009**, *47*, 145−152.
(26) Wood, S. M.; Pham, C. H.; Heller, A.; Mullins, C. B. Communication — Stages in the Dynamic Electrochemical Lithiation of Lead. *J. Electrochem. Soc.* **2016**, *163*, A1027−A1029.
(27) Peng, B.; Xu, Y.; Wang, X.; Shi, X.; Mulder, F. M. The electrochemical performance of super P carbon black in reversible Li/Na ion uptake. *Sci. China: Phys., Mech. Astron.* **2017**, *60*, 064611.


DOI: 10.1021/acsaem.9b00401
*ACS Appl. Energy Mater.* 2019, 2, 3017−3020